



A novel trigger algorithm for wide-field-of-view imaging atmospheric Cherenkov technique experiments

Guang-Guang Xin¹ · Hao Cai¹ · Yi-Qing Guo² · Tian-Lu Chen³ · Cheng Liu² · Xiang-Li Qian⁴

Received: 24 September 2021 / Revised: 16 December 2021 / Accepted: 16 December 2021 / Published online: 3 March 2022
© The Author(s), under exclusive licence to China Science Publishing & Media Ltd. (Science Press), Shanghai Institute of Applied Physics, the Chinese Academy of Sciences, Chinese Nuclear Society 2022

Abstract The high-altitude detection of astronomical radiation (HADAR) experiment is a new Cherenkov observation technique with a wide field of view (FoV), aimed at observing the prompt emissions of γ -ray bursts (GRBs). The bottleneck for this type of experiment can be found in determining how to reject the high rate of night-sky background (NSB) noise from random stars. In this work, we propose a novel method for rejecting noise, which considers the spatial properties of GRBs and the temporal characteristics of Cherenkov radiation. In space coordinates, the map between the celestial sphere and the fired photomultiplier tubes (PMTs) on the telescope's camera can be expressed as $f(\delta(i, j)) = \delta'(i', j')$, which means that a limited number of PMTs is selected from one direction. On the temporal scale, a 20-ns time window was

selected based on the knowledge of Cherenkov radiation. This allowed integration of the NSB for a short time interval. Consequently, the angular resolution and effective area at 100 GeV in the HADAR experiment were obtained as 0.2° and 10^4 m^2 , respectively. This method can be applied to all wide-FoV experiments.

Keywords IACTs · Wide field of view (FoV) · γ -ray burst · Cherenkov radiation

1 Introduction

γ -ray bursts (GRBs) are a phenomenon in which gamma rays from the depths of the universe suddenly increase on a short-time scale; they are the most violent explosion phenomenon after the Big Bang. Theoretically, the prompt emission of the GRB is generated by the energy dissipation process inside the relativistic jet, whereas the multi-band afterglow emission is generated by the external shock caused by the collision between the relativistic jet and the external medium. Therefore, gamma bursts are used to study the emergence of compact celestial bodies (black holes with constant star mass and neutron stars), gravitational wave radiation, relativistic shock waves, extremely high-energy cosmic rays, high-energy neutrinos, and other extreme objects in astronomical laboratories for scientific phenomena and high-precision testing of basic physical principles; they are also important probes for early universe star formation and evolution, high-redshift galaxies, and high-redshift cosmology.

The first γ -ray burst (GRB) was discovered by the Vela U.S. military satellites in 1967 and was recognized early as being of extrasolar origin [1]. A bimodal structure (first

This work was supported by the Key R&D Program of Sichuan Province (Nos. 2019ZYZF0001 and 2020YFSY0016) and the National Natural Science Foundation of China (Nos. 11873005, 12047575, 11705103, 11635011, U1831208, U1632104, 11875264, and U2031110).

✉ Hao Cai
hcai@whu.edu.cn

✉ Yi-Qing Guo
guoyq@ihep.ac.cn

- ¹ School of Physics and Technology, Wuhan University, Wuhan 430072, China
- ² Key Laboratory of Particle Astrophysics, Institute of High Energy Physics, Chinese Academy of Sciences, Beijing 100049, China
- ³ Ministry of Education, The Key Laboratory of Cosmic Rays (Tibet University), Lhasa 850000, China
- ⁴ School of Intelligent Engineering, Shandong Management University, Jinan 250357, China

reported in [2]) in the duration distribution of GRBs was detected by the Burst and Transient Source Experiment (BATSE) onboard the Compton Gamma Ray Observatory (CGRO) [3], based on which GRBs are currently commonly classified as short (with a duration $T_{90} < 2$ s, SGRBs) and long (with $T_{90} > 2$ s, LGRBs) [4]. BATSE observations have also confirmed that GRBs have an isotropic angular distribution in the sky [3, 5–8]. GRB970508, with $0.835 < z \leq 2.3$, was placed at a cosmological distance of at least 2.9 Gpc, which was later corroborated by the first redshift measurement [9]. Subsequently, the progenitors of LGRBs were associated with supernovae (SNe) [10–14] related to the collapse of massive stars. The first direct detection of gravitational waves (GWs) by the Laser-Interferometer Gravitational-Wave Observatory, termed GW150914, was interpreted as a merger of two stellar-mass black holes (BHs) with masses and was, by itself, a discovery of prime importance [15]. It became especially interesting in light of the discovery of a weak transient source lasting 1 s in [16] and detected by Fermi/GBM [17] only 0.4 s after the GW150914 (termed GW150914-GBM). The highest-energy GRB photon ever recorded by Fermi-LAT thus far had been emitted by GRB 130427A in the early afterglow phase and had an energy of 95 GeV (128 GeV in the rest frame during a redshift $z = 0.34$) [18]. While LAT-detected GRBs commonly exhibit photon energies of a few hundred MeV, higher energies are relatively rare. Although satellite experiments have provided a vast number of exciting results, they are limited by their effective areas and have difficulty detecting higher-energy photons in the prompt emissions of GRBs.

Recently, sub-TeV energy γ rays were successfully observed by the Major Atmospheric Gamma Imaging Cherenkov (MAGIC) and High Energy Stereoscopic System (H.E.S.S.) telescopes approximately 1 min after the GRB 190114C burst and 10 h after the end of the prompt-emission phase of GRB 180720B [19–21]. These events were unique, as researchers were able to observe them for the first time in afterglow emission photons with sub-TeV energies. Soon thereafter, the H.E.S.S. collaboration announced the detection of photons with energies up to 4 TeV high from GRB 190829A between 4 h and 56 h after the trigger [22]. Additionally, MAGIC reported the detection of hundreds of GeV γ -ray emissions from GRB 201216C in the afterglow phase [23]. Along with GRB 160821B and GRB 201015A, from which over 100 GeV of emissions at the $\leq 3\sigma$ level have been reported [24, 25], six GRBs have been reported with VHE afterglow emissions. Imaging atmospheric Cherenkov telescopes (IACTs) have been making great progress in the observations of VHE emissions in the afterglow phase. However, it is

challenging for IACTs to conduct prompt-phase observation. They have a narrow field of view (FoV) and need to slew because a GRB does not typically enter their FoV within the first seconds of the prompt phase occurring, even if they have larger effective areas (unless the GRB occurs in their FoV, which has a very small probability).

Traditional extended air shower (EAS) experiments, for example, the High-Altitude Water Cherenkov Observatory [26] and the Large High Altitude Air Shower Observatory [27], which have wide FoVs, high duty cycles, and large effective areas, have not yet detected GRBs. In general, the energy thresholds of the EAS experiments are also higher than those of the IACT experiments.

The detection of high-energy photons in the prompt phase of the GRB is conducive to understanding the acceleration mechanisms and energetics because it constrains the progenitors, jet feeding mechanism, and extragalactic background light (EBL)-induced absorption of high-energy photons, which limits the Lorentz invariance violation (LIV). Therefore, it is important to search for prompt VHE emissions from GRBs using ground-based instruments that can achieve excellent sensitivity and a low-energy threshold over a wide FoV. The high-altitude detection of astronomical radiation (HADAR) experiment is a new observation instrument that uses a large-dimensional refractive water lens as a light collector to observe Cherenkov light induced by VHE cosmic rays (CRs) and γ rays in the atmosphere. In 2016, a prototype experiment was conducted and was successfully operated at the Yangbajing Observatory (4300 m above sea level, 90.522° E, 30.102° N, 606 g/cm^2) in Tibet, China. Cosmic rays were successfully detected. More detailed information is available in [28, 29].

However, the bottleneck in wide-FoV Cherenkov technology is caused by the high rate of night-sky background (NSB) noise from random stars overwhelming the Cherenkov light signal from a GRB. Consequently, images of air showers recorded by telescopes are indistinguishable, and the fitting of a Hillas ellipse with the fired photomultiplier tubes (PMTs) on the camera, a critical step in event reconstruction, cannot be precisely performed. In this study, we propose a novel method that considers the spatial properties of GRBs and the temporal characteristics of Cherenkov radiation to reject NSB noise.

The remainder of this paper is organized as follows. Section 2 describes the HADAR experiment in detail. Section 3 presents a novel trigger method for wide-view IACT experiments, and Sect. 4 includes the results of the novel trigger method. Section 5 presents the conclusions of the study.

2 Imaging atmospheric Cherenkov technique and the HADAR experiment

2.1 Imaging atmospheric Cherenkov technique (IACT)

Cherenkov radiation is produced when an energetically charged particle moves through a dielectric medium at a velocity higher than the speed of light. The electric field of the particle polarizes the adjacent molecules in the medium. Once the particle has passed, the molecules return to their original dipole configuration by releasing a brief pulse of continuum electromagnetic radiation that peaks at the UV and blue wavelengths.

The radiation fans out in the shape of a cone along the direction of the particle's path. The emission of molecules in the wake of the particle interferes constructively via the Huygens-Fresnel principle. The opening angle of this cone for a medium with refractive index n is given by

$$\cos \theta_C = \frac{(\frac{c}{n})t}{v_s t} = \frac{c}{nv_s}, \quad (1)$$

where angle θ_C is known as the Cherenkov angle, v_s is the speed of the particle, and c is the speed of light in a vacuum.

The change in the refractive index n as a function of atmospheric depth means that the light pool at the ground level takes the shape of a flattened disk or pancake. When a γ -ray above 1.022 MeV ($2M_{e^+e^-}$) interacts with the nucleus of an oxygen or nitrogen atom in the upper atmosphere, it spontaneously produces electron-positron pairs. Conservation of momentum dictates that these particles travel close to the incident direction of the γ -ray at nearly the speed of light, thereby producing Cherenkov radiation in their wake above the threshold energy. γ rays are not the only sources of particle showers in the atmosphere. Cosmic rays that pass through the atmosphere also induce extensive air showers (EASs).

The method for imaging Cherenkov radiation in the atmosphere consists of a large optical collection dish comprising tessellated mirror facets focused onto a multi-pixel camera box. The pixels contain PMTs that can register single photons with a time resolution comparable to that of Cherenkov flash (a few nanoseconds). The PMTs and their associated back-end electronics record images of the air shower as a signal above the ambient night-sky background in real time as it progresses; when the radiation reaches the ground, its intensity is quite faint, only 100 photons/m² originating from a 1 TeV γ ray; therefore, multiple imaging atmospheric Cherenkov telescopes (IACTs) are often evenly distributed around a site to maximize the effective area of the array.

2.2 HADAR experiment

The HADAR instrument was configured with four water-lens telescopes that employed the imaging atmospheric Cherenkov technique, whose main task is to measure Cherenkov light induced by 10 GeV to 100 TeV CRs and γ rays in the atmosphere. The four water-lens telescopes were square-shaped with a side length of 100 m. The side length was selected because the Cherenkov light pool generally has a radius of approximately 125 m [30]. To perform joint observations, plastic scintillation detectors of the Yangbajing hybrid array were added to the telescope system. A water-lens telescope consists mainly of an acrylic spherical cap lens with a diameter of 5 m, a cylindrical tank with a radius of 4 m and a height of 7 m, and a camera with an array of 18961 PMTs with 5 cm diameters. The steel tank, containing an absorption layer in the inside wall and a thermal insulation material coated on the outer wall, is filled with purified water to reflect radiation emissions to the PMTs. The PMTs are placed in the focal plane of the lens and arranged as a series of concentric ring matrices supported by a stainless steel space frame. The details of the profile structure of a water-lens telescope and the instrument layout can be found in [31].

Focal length (FL) is one of the most important parameters of a lens. The value of the FL measured by ZEMAX was $F_{\text{exp}} = 690 \pm 1.5$ cm [32]. The parameters used in the ZEMAX simulation were the same as the geometric parameters of the lens. Thus, the focal ratio $N = F/\Phi = 1.38$. As a pathfinder experiment, the HADAR was designed to explore the processing technique of a wide FoV water lens. Hence, we chose a commercial material, acrylic, as the shell of the prototype water lens instead of high-UV-transparent materials. The absorption of acrylic and purified water can be ignored in the water-lens optical system at wavelengths between 400 nm and 500 nm. Because the camera did not occlude the lens, the telescope could obtain a wide FoV for observation. The camera was designed on a curved surface to ensure that the light incident at a large angle could be clearly focused. The light parallel to the main optical axis of the telescope at 0-30° was well focused.

3 Trigger algorithm

GRB jets are usually unresolved and are viewed as point sources by instruments that are observational rather than intrinsic. This is because of their intrinsically small size, especially at early times, and their cosmological distances, which result in very small angular sizes [33]. Therefore, the GRB signal exhibits spatial characteristics. The main

high-rate noise is NSB noise, which is emitted from random stars because IACTs can only make observations on clear and moonless nights. In contrast, NSB is isotropic and has no spatial characteristics.

Generally, H.E.S.S. or MAGIC telescopes are equipped with a large optical reflecting dish. These telescopes must rotate with the gamma source when they make scientific observations because they have a narrow FoV. However, owing to the small FoV, the night sky background noise received by the mirror is significantly lesser. After a simple cut on pixels (e.g., image cleaning), a clearer Cherenkov image caused by CR or γ rays can be obtained on the camera. However, this trigger method cannot be directly applied to experiments with a wide FoV, such as the HADAR. Because HADAR telescopes have a wide FoV, this introduces a significant amount of NSB noise. The challenge for the HADAR experiment is determining how to reject the high rate of NSB noise from random stars. For high-energy events, the effect of the NSB noise can be ignored because high-energy events generate many Cherenkov photons. The signal is not overwhelmed by the noise. However, low-energy events do not generate as many photons as high-energy events. It is difficult to distinguish which PMTs have been triggered by noise, and which have been triggered by Cherenkov photons. Clear images cannot be obtained. Therefore, to make better scientific observations using HADAR, we improved the trigger method.

As shown in Fig. 1, on a clear and moonless night, a GRB appeared at $\delta(i, j)$ on the celestial sphere, which was in the FoV of the HADAR experiment. High-energy γ rays from the GRB entered and interacted with the Earth's

atmosphere. They produced a large number of electron-positron pairs with enormous velocities. When electron-positron pairs travel faster than light in the Earth's atmosphere, their passage causes a brief flash of light: Cherenkov light. The photons from the Cherenkov radiation were collected by the lens and focused on by the camera (this was the signal of interest). Simultaneously, the photons from the random stars also entered the lens and were recorded by the camera (this was the main noise). At low energy, the crucial signals from the GRB were submerged by NSB noise.

The trigger algorithm used by HADAR was as follows: (1) one PMT was fired if ≥ 9 photoelectrons were collected by the PMT within the time window; (2) if the number of adjacent triggered PMTs on the camera was $n \geq 3$, a telescope was considered to be triggered; (3) an event was recorded if ≥ 2 telescopes were triggered in a time window of 20 ns (to reconstruct the event); (4) a 10×10 PMT matrix was selected from the camera with adjacent triggered PMTs as the center. Subsequently, all fired PMTs in the matrix were used to fit the Hillas ellipse (a key step for event reconstruction). The area enclosed by the ellipse is denoted as $\delta'(i', j')$. Other PMTs outside the matrix were masked to reduce the trigger rate of the NSB noise. As previously mentioned, GRBs have distinct spatial properties. Therefore, to perform detection even at low energies, a map between $\delta(i, j)$, the position of the GRB on the celestial sphere, and $\delta'(i', j')$, where the signals were large and concentrated on the camera, could be constructed as follows: $f(\delta(i, j)) = \delta'(i', j')$. This implies that a limited number of PMTs were selected from one direction.

Because the atmospheric index of refraction was very close to 1, the Cherenkov light almost kept pace with radiating charged particles. Near the edge of the "light pool", most of the light from the γ ray shower arrived within 2 ns. Thus, a very short temporal window was possible, allowing for suppression of the dominant NSB. The number of background photons is given as follows:

$$n_{\text{ph}} = BA\Omega\xi\tau, \tag{2}$$

where B is $557 \text{ m}^{-2}\text{sr}^{-1}\text{ns}^{-1}$, A is the mirror area (in this study, $A \approx 43 \text{ m}^2$), Ω is the solid angle corresponding to each PMT ($\Omega \approx 1.6 \times 10^{-4} \text{ sr}$), ξ is the photocathode quantum efficiency, and τ is the integration time of $\approx 20 \text{ ns}$. The number of Cherenkov photons is given as follows:

$$N_{\text{ph}} = NA\xi, \tag{3}$$

where N is the number of Cherenkov photons per m^{-2} inside the solid angle Ω at a given distance from the shower axis. In the integration temporal window of $\tau = 20 \text{ ns}$, the Cherenkov signal was fully recorded, while introducing as

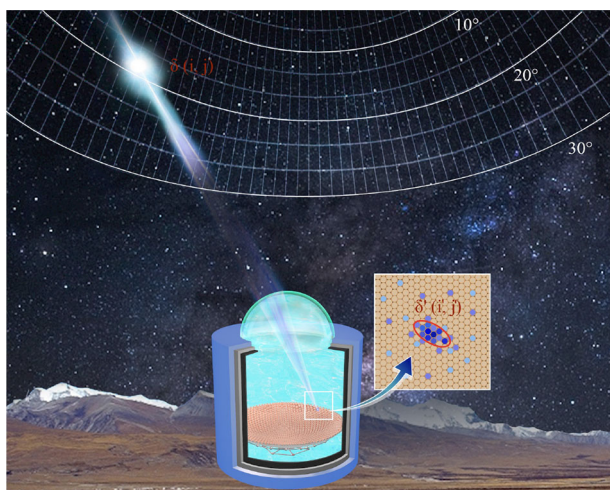


Fig. 1 (Color online) Mapping the location where there was a GRB on a celestial sphere with a fired PMT on the camera. $\delta(i, j)$ denotes the position of the GRB on the celestial sphere. $\delta'(i', j')$ is the area where the signal is stronger and concentrated in the camera (circled by the red ellipse)

little noise as possible. This suggests the use of fast photomultiplier cameras in telescopes for this purpose.

4 Result

After applying the new trigger method, the NSB was suppressed and the angular resolution and effective area were significantly improved.

In Fig. 2, the black line represents the time distribution of all photons (including NSB and Cherenkov photons) received by all PMTs. The NSB overwhelmed the Cherenkov signals of interest. After selecting the area $\delta'(i', j')$ with the strongest signal on the camera (blue line), the NSB was suppressed, and the Cherenkov signal was well preserved compared to the case that only included Cherenkov photons (red line).

In addition, the angular resolution was improved and the effective area increased. Fitting a Hillas ellipse is a critical step for event reconstruction in IACTs. However, while applying all PMTs of one camera, it becomes a challenge to fit a Hillas ellipse with fired PMTs because many of them are fired by the NSB. This results in a significant difference between the reconstructed and real directions. Therefore, the angular resolution was $> 1^\circ$ at $E < 200$ GeV, as indicated by the black line in Fig. 3, when applying all PMTs of one camera. As the energy increased, the angular resolution gradually approached 1° . This was because the Cherenkov signals became stronger and were no longer submerged by the NSB. The angular resolution improved considerably after selecting $\delta'(i', j')$ on the camera, as

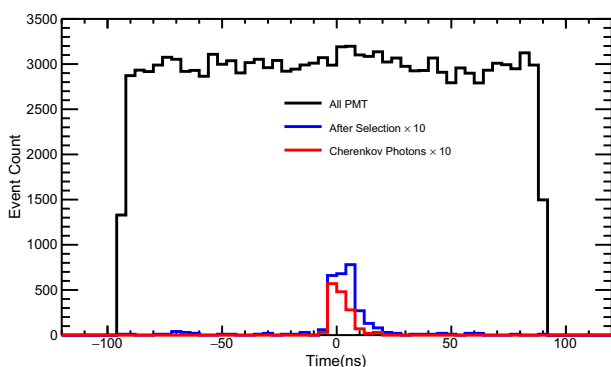


Fig. 2 (Color online) Time distribution of photons received by the PMT. The black line represents the time distribution of all photons (including the NSB and Cherenkov photons) received by all PMTs. The blue line represents the time distribution of photons, including a small number of NSB photons and most Cherenkov photons after selecting $\delta'(i', j')$ on the camera. The red line represents the time distribution containing only the Cherenkov photons. To demonstrate this more clearly, the selection and Cherenkov distributions were both scaled by 10

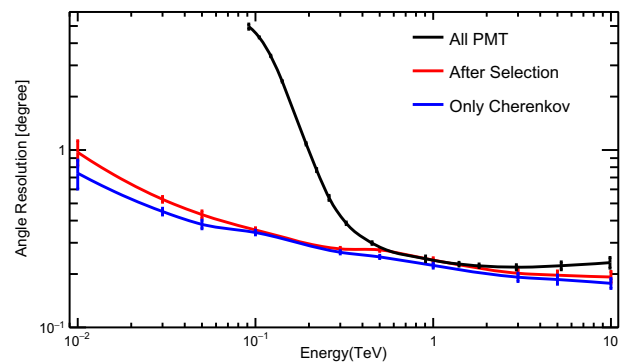


Fig. 3 (Color online) Angular resolution. Black line: application of all PMTs to the camera. Red line: after selection. Blue line: only Cherenkov photons

indicated by the red line. After selection, the fired PMTs could be fitted by a qualified ellipse that contained the essential parameters for event reconstruction at low energy. Furthermore, the angular resolution of the high-energy event was also improved. In contrast to the blue line, which corresponds to the case with only Cherenkov photons, the red line indicates that the NSB has a certain influence on the event reconstruction.

Figure 4 shows the effective area of the HADAR experiment. The simulated area was 800×800 m². The black line was the effective area before PMT selection. At $E < 200$ GeV, almost every event triggered the telescope array because the NSB was introduced heavily, resulting in many PMTs being fired. After PMT selection, because the NSB was suppressed and Cherenkov photons were lower in low energy, the probability of event triggering the telescope array became lower, which was almost the same as the case with only Cherenkov photons, as shown by the red and blue lines. Aside from the angular resolution, when $E > 300$ GeV, the effective area was almost the same in the three cases.

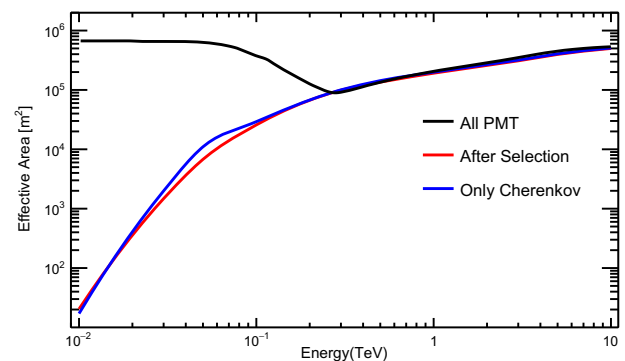


Fig. 4 (Color online) Effective area. Black line: application of all PMTs to the camera. Red line: after selection. Blue line: only Cherenkov photons

5 Conclusion

Unlike the afterglow theory, which is relatively simple and well-tested by data, the GRB prompt-emission theory is much more complicated. Thus, more experimental data are required for prompt GRB emissions. The HADAR experiment provides an effective solution for detecting GRB prompt emissions on the ground. Unlike satellite experiments with small effective areas and traditional IACTs with narrow FoVs, the HADAR experiment has a large effective area and wide FoV. The wide FoV allows telescopes to cover a larger area of the celestial sphere and observe GRBs without slewing. However, a wide FoV introduces considerable noise from the NSB, making it difficult to observe low-energy events.

To solve this problem, the GRB's spatial properties and temporal structure of atmospheric Cherenkov radiation were fully utilized. At the coordinates $\delta'(i', j')$, a stronger and concentrated signal on the camera was selected and mapped to $\delta(i, j)$, the position of the GRB on the celestial sphere. To fully record the Cherenkov signal while introducing as little noise as possible, a 20-ns integration temporal window was selected. After applying the new trigger method, the angular resolution of low-energy events significantly improved, and the angular resolution was 1° at 10 GeV. Moreover, the trigger rate of the telescope array was significantly reduced at low energy because the NSB noise was suppressed. This method can be used in all the wide-FoV IACT experiments. As the angular resolution and effective area of HADAR have improved, HADAR's capacity to observe GRBs increases the detection rate to at least one GRB per year. We hope that future experimental observations can confirm the progress of physics in the prompt phase and relevant parameters.

Author Contributions All authors contributed to the study conception and design. Material preparation, data collection and analysis were performed by Hao Cai, Yi-Qing Guo and Guang-Guang Xin. The first draft of the manuscript was written by Guang-Guang Xin and all authors commented on previous versions of the manuscript. All authors read and approved the final manuscript.

References

1. R.W. Klebesadel, I.B. Strong, R.A. Olson, Observation of gamma-ray bursts of cosmic origin. *Astrophys. J.* **182**, 85–88 (1973). <https://doi.org/10.1086/181225>
2. E.P. Mazets, S.V. Golenetskii, V.N. Il'inskiĭ et al., Catalog of cosmic gamma-ray bursts from the KONUS experiment dataparts I and II. *Astrophys. Space Sci.* **80**, 3–83 (1981). <https://doi.org/10.1007/BF00649140>
3. C.A. Meegan, G.J. Fishman, R.B. Wilson et al., Spatial distribution of gamma-ray bursts observed by BATSE. *Nature* **355**, 143–145 (1992). <https://doi.org/10.1038/355143a0>
4. C. Kouveliotou, C.A. Meegan, G.J. Fishman et al., Identification of two classes of gamma-ray bursts. *Astrophys. J.* **413**, 101–104 (1993). <https://doi.org/10.1086/186969>
5. B. Paczynski, A test of the galactic origin of gamma-ray bursts. *Astrophys. J.* **348**, 485–494 (1990). <https://doi.org/10.1086/168257>
6. B. Paczynski, Cosmological gamma-ray bursts. *Acta Astron.* **41**, 257–267 (1991)
7. G.J. Fishman, γ -ray bursts. *Annu. Rev. Astron. Astrophys.* **33**, 415–458 (1995). <https://doi.org/10.1146/annurev.aa.33.090195.002215>
8. M.S. Briggs, W.S. Paciesas, G.N. Pendleton et al., BATSE observations of the large-scale isotropy of gamma-ray bursts. *Astrophys. J.* **459**, 40 (1996). <https://doi.org/10.1086/176867>
9. M.R. Metzger, S.G. Djorgovski, S.R. Kulkarni et al., Spectral constraints on the redshift of the optical counterpart to the γ -ray burst of 8 May 1997. *Nature* **387**, 878–880 (1997). <https://doi.org/10.1038/43132>
10. J. Hjorth, J. Sollerman, P. Møller et al., A very energetic supernova associated with the γ -ray burst of 29 March 2003. *Nature* **423**, 847–850 (2003). <https://doi.org/10.1038/nature01750>
11. D. Malesani, G. Tagliaferri, G. Chincarini et al., SN 2003lw and GRB 031203: a bright supernova for a faint gamma-ray burst. *Astrophys. J.* **609**, L5–L8 (2004). <https://doi.org/10.1086/422684>
12. S.E. Woosley, J.S. Bloom, The supernova-gamma-ray burst connection. *Annu. Rev. Astron. Astrophys.* **44**, 507–556 (2006). <https://doi.org/10.1146/annurev.astro.43.072103.150558>
13. M. Sparre, J. Sollerman, J.P.U. Fynbo et al., Spectroscopic evidence for SN 2010ma associated with GRB 101219B. *Astrophys. J. Lett.* **735**, L24 (2011). <https://doi.org/10.1088/2041-8205/735/1/L24>
14. S. Schulze, D. Malesani, A. Cucchiara et al., GRB 120422A/SN 2012bz: bridging the gap between low- and high-luminosity gamma-ray bursts. *Astron. Astrophys.* **566**, A102 (2014). <https://doi.org/10.1051/0004-6361/201423387>
15. B.P. Abbott, R. Abbott, T.D. Abbott et al., Observation of gravitational waves from a binary black hole merger. *Phys. Rev. Lett.* **116**, 061102 (2016). <https://doi.org/10.1103/PhysRevLett.116.061102>
16. V. Connaughton, E. Burns, A. Goldstein et al., Fermi GBM observations of ligo gravitational-wave event GW150914. *Astrophys. J. Lett.* **826**, L6 (2016). <https://doi.org/10.3847/2041-8205/826/1/L6>
17. P.N. Bhat, C.A. Meegan, A. Von Kienlin et al., The third fermi GBM gamma-ray burst catalog: the first six years. *Astrophys. J. Suppl. Ser.* **223**, 28 (2016). <https://doi.org/10.3847/0067-0049/223/2/28>
18. M. Ackermann, M. Ajello, K. Asano et al., Fermi-LAT Observations of the Gamma-Ray Burst GRB 130427A. *Science* **343**, 42–47 (2014). <https://doi.org/10.1126/science.1242353>
19. MAGIC Collaboration, V.A. Acciari, S. Ansoldi et al., Observation of inverse Compton emission from a long γ -ray burst. *Nature* **575**, 459–463 (2019). <https://doi.org/10.1038/s41586-019-1754-6>
20. MAGIC Collaboration, V.A. Acciari, S. Ansoldi et al., Teraelectronvolt emission from the γ -ray burst GRB 190114C. *Nature* **575**, 455–458 (2019). <https://doi.org/10.1038/s41586-019-1750-x>
21. H. Abdalla, R. Adam, F. Aharonian et al., A very-high-energy component deep in the gamma-ray burst afterglow. *Nature* **575**, 464–467 (2019). <https://doi.org/10.1038/s41586-019-1743-9>
22. H.E.S.S. Collaboration, H. Abdalla, F. Aharonian et al., Revealing x-ray and gamma ray temporal and spectral similarities in the GRB 190829A afterglow. *Science* **372**, 1081–1085 (2021). <https://doi.org/10.1126/science.abe8560>

23. C. Malacaria, P. Veres, C. Meegan et al., GRB 201216C: Fermi GBM detection. GRB Coordinates Network, Circular Service, No. 29073 (2020)
24. MAGIC Collaboration, V.A. Acciari, S. Ansoldi et al., MAGIC observations of the nearby short gamma-ray burst GRB 160821B. *Astrophys. J.* **908**, 90 (2021). <https://doi.org/10.3847/1538-4357/abd249>
25. O. Blanch, M. Gaug, K. Noda et al., MAGIC observations of GRB 201015A: hint of very high energy gamma-ray signal. GRB Coordinates Network, No. 28659 (2020)
26. R.W.Springer for the HAWC Collaboration, The high altitude water Cherenkov (HAWC) observatory. *Nucl. Part. Phys. Proc.* **279-281**, 87–94 (2016) <https://doi.org/10.1016/j.nuclphysbps.2016.10.013>
27. X.Y. Wang, X.J. Bi, Z. Cao et al., Chapter 3 Extra-galactic gamma-ray sources. *Chinese Phys. C* **46**, 030003 (2022). <https://doi.org/10.1088/1674-1137/ac3fa9>
28. H. Cai, Y. Zhang, C. Liu et al., Wide field-of-view atmospheric Cherenkov telescope based on refractive lens. *J. Instrum.* **12**, P09023 (2017). <https://doi.org/10.1088/1748-0221/12/09/p09023>
29. T.L. Chen, C. Liu, Q. Gao et al., Performance of a wide field-of-view atmospheric Cherenkov telescope prototype based on a refractive lens. *Nucl. Instrum. Methods. Phys. Res. A* **927**, 46–53 (2019). <https://doi.org/10.1016/j.nima.2019.02.020>
30. H.J. Voelk, K. Bernloehr, Imaging very high energy gamma-ray telescopes. *Exp. Astron.* **25**, 173–191 (2019). <https://doi.org/10.1007/s10686-009-9151-z>
31. G.G. Xin, Y.H. Yao, X.L. Qian et al., Prospects of γ -ray bursts detecting at very high energy with the High Altitude Detection of Astronomical Radiation experiment. <https://doi.org/10.3847/1538-4357/ac2df7>
32. ZEMAX homepage, <https://www.zemax.com>
33. J. Granot, A.J. van der Horst, Gamma-ray burst jets and their radio observations. *Public. Astron. Soc. Australia* **31**, E008 (2014). <https://doi.org/10.1017/pasa.2013.44>